Thermal and Electrical Energy Transport and Conversion in Nanoscale Electron Field Emission Processes

T. S. Fisher
e-mail: tsfisher@purdue.edu
Purdue University,
School of Mechanical Engineering,
1288 Mechanical Engineering Building,
West Lafayette, IN 47907-1288

D. G. Walker
Vanderbilt University
Department of Mechanical Engineering,
Box 1592, Station B,
Nashville, TN 37235

This paper considers the theory of electron field emission from nanoscale emitters with particular focus on thermal and electrical energy transport. The foundational theory of field emission is explored, and a model is presented that accounts explicitly for the energy band curvature produced by nanoscale tip emitters. The results indicate that the inclusion of band curvature strongly influences the energetic distribution of electrons for emitter radii less than 50 nm. The energy exchange process between emitted and replacement electrons is shown to allow high local energy transfer rates that can be exploited in direct thermal-to-electrical energy conversion processes. The dependence of energy conversion rates on material and operational parameters is demonstrated. Throughout the paper, opportunities for further research involving nanoscale heat transfer, materials development, and modeling are highlighted. [DOI: 10.1115/1.1494091]

Keywords: Electronics, Energy Conversion, Heat Transfer, Microscale, Nanoscale

1 Introduction

Prolific advances in microscale and nanoscale technologies have generated renewed scientific interest in direct thermal-to-electrical energy conversion. These advances have provided researchers with new tools to explore physical phenomena that were previously inaccessible. For example, the controlled fabrication of one- and two-dimensional nanoscale structures has fostered significant recent improvements in the efficiency and capacity of thermoelectric materials and devices [1,2]. Further, the development of thin-film heterostructures has brought thermionic energy conversion, originally a vacuum-based technology, to the solid state [3,4]. The phenomenon of electron field emission is, in some respects, similar to thermoelectric and thermionic transport. However, the thermodynamics of field emission have received less attention, although several recent theoretical papers on direct refrigeration suggest that field emission devices could operate remarkably well [5–10]. In the present work, we consider the foundations of and prospects for direct energy conversion by electron field emission and show that outstanding performance is possible with further progress in fabrication technology, modeling, and engineering.

The emission of electrons from an electrically active surface via quantum tunneling into a vacuum is commonly referred to as field emission. Fowler and Nordheim [11] provided the first theoretical treatment of field emission from planar metal surfaces. Later studies showed that emission could be substantially improved by geometric electric field enhancement provided by elongated structures, such as pyramidal or conical tips. Spindt was the first to show such enhancement using molybdenum cones [12]. Since then, the emission properties of a wide variety of metallic and semiconductor materials and structures have been studied in detail [13,14]. The emission properties of carbon-based/diamond materials, in particular, are very robust [15]. Because they do not require heating, carbon-based and other field emitters are often termed cold cathodes. However, the physical reasons behind the outstanding emission properties of carbon-based materials remain the subject of scientific inquiry [16]. Suggested applications for field emission devices include vacuum field-effect transistors, diodes and triodes, ion sources, electron guns, flat-panel displays, scanning microscopes, and many others [13].

Field emission devices are formed by placing an emitting cathode in close proximity to an anode, separated by vacuum (typically less than 10^{-5} torr). A gate electrode may also be included to modulate emission and to provide a more precise spatial separation from the cathode. Figure 1 shows a tip configuration. The cathode, anode and base electrode materials can be semiconductor (with narrow or wide band gaps) or metals. The gate is typically metallic, and the dielectric between the cathode and gate is commonly SiO_2. Field emission occurs when a sufficiently strong *local* electric field (greater than 0.5 V/Å) exists at the location of emission. Small-scale features within a low average electric field can produce a high local field. Cathode tip structures are designed to provide this field enhancement. Some field enhancement also occurs in film cathodes due to highly localized areas of emission [13].

Most prior work has focused on device operation near room temperature. In fact, the predominant theoretical foundation of field emission—basic Fowler-Nordheim theory—neglects the effects of temperature on emission characteristics. In contrast, consideration of the thermodynamics of field emission requires the inclusion of temperature effects. Fleming and Henderson [17] conducted early experiments on the energy distribution of field-emitted electrons. Their work prompted an exchange of letters with Nottingham [18,19], who predicted that field emission could produce a heating or cooling effect on the cathode, depending on the field strength. Subsequent studies by Good and Muller [20], Dyke and Dolan [21], and Gomer [22] provided a more detailed treatment of the thermodynamics of field emission.

After these early studies, relatively little work occurred on the thermodynamics of field emission for several decades. However, studies by Swanson et al. [23], Engle and Cutler [24], and Bergeret et al. [25] considered measurements of the so-called Nottingham effect [23,25] and the thermodynamics of electron emission and replacement processes [24]. In the past decade, Cutler, Miskovsky, and co-workers have studied various facets of thermodynamics in field emission processes, particularly from diamond

Contributed by the Heat Transfer Division for publication in the JOURNAL OF HEAT TRANSFER. Manuscript received by the Heat Transfer Division May 2, 2001; revision received November 5, 2001. Associate Editor: A. Majumdar.

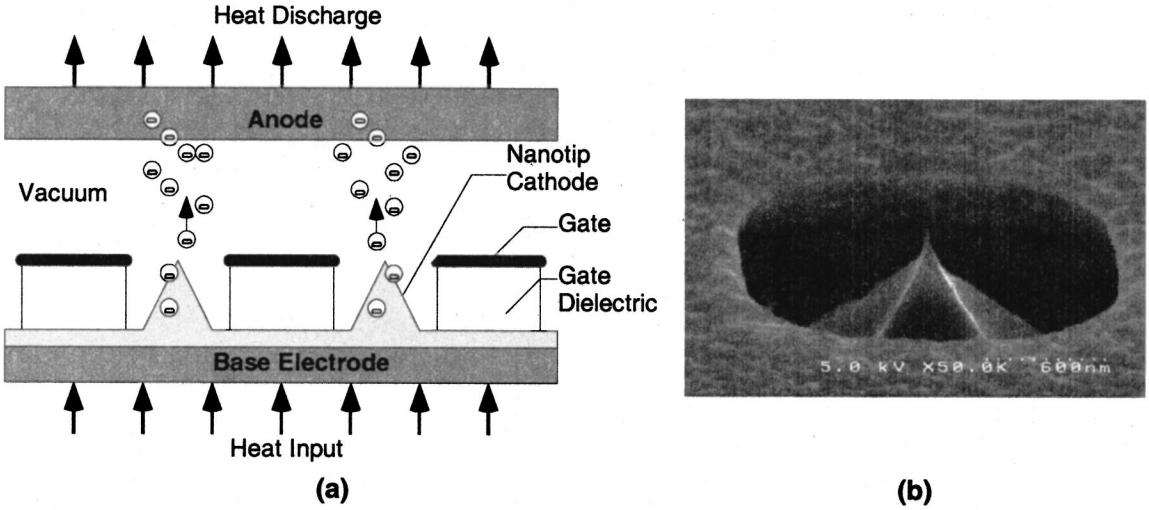

Fig. 1 Nanotips for electron field emission: (*a*) Schematic of an energy conversion system including nanotip electron emitters (cathode), gate electrode, and anode; and (*b*) Example of a polycrystalline diamond nanotip emitter surrounded by a monolithic gate. The tip radius is ~10 nm.

films, including: cathode heating mechanisms and energy exchange processes in sharp metallic emitters [26], average electron energies of emission and replacement [27,28], effects of doping [29], ballistic electron transport [30,31], and internal field emission [32–34]. This body of work has significantly advanced the theoretical understanding of energetic processes in field emission. Yet, the complexity of the physical processes involved in field emission, particularly from polycrystalline materials such as chemical vapor deposited (CVD) diamond, has prevented a thorough understanding of experimentally observed phenomena. Such understanding will be essential if the promise of energy conversion by electron field emission is to be realized.

In the present work, we review the foundational theory of nanoscale field emission with an emphasis on energy transport processes and modeling. The simplifying assumptions that are central to traditional field emission theory are presented, and their applicability to thermodynamic modeling is considered in detail. A more accurate model, which explicitly accounts for emitter-size effects and temperature dependence, is presented for thermodynamic calculations. This model is exercised over relevant parameter ranges, and its utility in interpreting experimental data is demonstrated. This work does not focus on specific energy conversion devices and systems, but rather, provides new insights into energy transport mechanisms in electron field emission from nanoscale emitters. Throughout the work, we identify opportunities for further improvements in modeling and experimental methods and highlight applications to heat transfer and energy conversion that will be important to the future development of nanoscale thermodynamic field emission devices.

2 Thermodynamics of Field Emission

2.1 The Field Emission Process. Field emission occurs when electrons tunnel through a sufficiently narrow potential barrier created by the application of a voltage bias between a cathode (negative bias) and an anode or gate electrode (positive bias). Fowler and Nordheim presented the first theory of field emission from a planar metal surface over seventy years ago [11]. Application of a voltage between planar electrodes creates a constant electric field $F=V/L$ (modified slightly by the image charge as discussed later), where V is the applied voltage and L is the distance between the electrodes. Emission from small, non-planar tips can substantially reduce the required field to produce emission by enhancing the *local* field near the emission site. This enhancement has traditionally been described within the framework of the planar field emission model by multiplying the applied field F by a field enhancement factor β [13–15] such that the local field at the tip becomes βF where β is greater than 1.

The field enhancement factor β depends strongly on small-scale structure. For tip emitters, electric field theory indicates that β is proportional to the inverse of the tip radius R [35]. Thus, the tip radius should be as small as possible to achieve low-voltage emission. However, the use of the field enhancement factor may not be appropriate for energy conversion studies. In effect, the field enhancement factor β linearizes the highly non-linear electric field near the emission surface, as illustrated in Fig. 2. In the figure, both the actual and linearized fields produce the same emission current by assumption. The linear field is necessary to arrive at the analytic current-field relation described below as the basic Fowler-Nordheim relation [see Eq. (7)]. However, the linearization does not satisfy the anode-side boundary condition on the electric potential and generally underestimates the emission flux of high-energy electrons (above the Fermi energy in Fig. 2) and overestimates the emission flux at energies below the Fermi level.

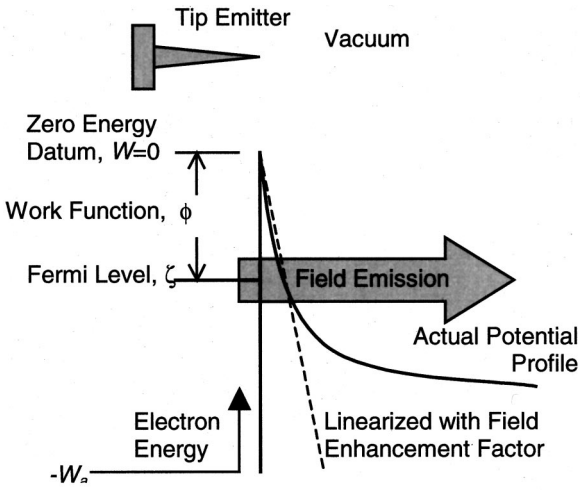

Fig. 2 Electron potential profile near a tip emitter. Solid line represents actual potential field. Dashed line represents approximate, linearized field. Both fields produce the same emission current.

For rectangular barriers, the probability of tunneling is inversely proportional to the exponential of the local potential barrier width [36]. Thus, the shape of the potential profile (which depends on the tip geometry) has a profound effect on the energy distribution of emitted electrons. Nanoscale tips produce extremely large curvature in the vacuum potential near the emission site. Tip radii of 5 nm have been reported [15]. The electrode spacing must be small to provide efficient emission and to minimize space-charge effects, which can degrade performance [37]. The combination of small tip radius R and electrode spacing can produce high emission with low applied bias. Thus, these small-scale features are essential in producing efficient, high-capacity thermal-electrical energy conversion.

In the present work, we employ a model that is more physically accurate than the basic Fowler-Nordheim approach. The present model allows for curvature of the potential field (such as shown in Fig. 2) and thus provides more accuracy in simulating the thermodynamics of field emission. Other more detailed models have been proposed [38–40], but these have typically focused on electronic applications and thus simplified the thermal considerations that are central to the present work. The one-dimensional model is based on the potential field in a spherically symmetric ball-shell system [[9,22] pp. 37–38] and takes the form:

$$V(x) = -qF(L+R)\left[1 - \frac{R}{x+R}\right] + G(x) \tag{1}$$

where q is the magnitude of electron charge, F is the applied (global) field, L is the separation distance between electrodes (taken as $L = 4\ \mu$m for all cases considered later), R is the *characteristic* radius of the emitter, x is the distance from the emitter, and $G(x)$ is the image potential experienced by emitting electron. This image potential for a spherical emitter tip can be expressed as [39]:

$$G(x) = \frac{-q^2}{4\pi\varepsilon_0}\frac{K-1}{K+1}\frac{R}{(2R+x)2x} \tag{2}$$

where ε_0 is permittivity of vacuum, and K is the emitter's dielectric constant. We note that this image potential neglects possible effects of surface plasmons on the tunneling electrons [41]. Subsequent results will show that the emitter radius R strongly influences the electrical and thermodynamic characteristics of field emission. The first term of Eq. (1) represents the contribution due to the applied field F and equals zero at the emission site ($x = 0$). Thus, following the formalism of Good and Muller [20], the zero energy datum exists at the cathode/vacuum interface of Fig. 2 (ignoring image charge potential). The second term in Eq. (1) represents the shift in potential due to image charge [20].

2.2 Current-Voltage Behavior. The physics of field emission have been described in detail by Good and Muller [20]. The development below provides some of the major results that are central to the present work. The total emission current density J takes the form

$$J = q\int_{-W_a}^{\infty} D(W)N(W)dW \tag{3}$$

where $-W_a$ represents the bottom of the emitter's conduction band, W is the x-component of electron energy (i.e., in the direction of emission), the term $N(W)dW$ is the electron supply function, and $D(W)$ is the quantum tunneling transmission coefficient. In the present work, the transmission coefficient is calculated using the WKB approximation [42]

$$D(W) = \exp\left\{-\int_{x_1}^{x_2}\sqrt{\frac{8m}{\hbar^2}|V(x)-W|}dx\right\} \tag{4}$$

where $V(x)$ is the potential profile [see Eq. (1)], x_1 and x_2 are the zeros of $W - V(x)$, and m is the mass of an electron. We note that the WKB approximation is, in general, limited to relatively low fields; however, this approximation is retained here for the purpose of obtaining results without the need to solve Schrödinger's equation numerically for each geometric and field condition. The effect of nanoscale features on the emission current is included through the energy profile $V(x)$ in the transmission coefficient of Eq. (4). The supply function, which represents the number of electrons whose x-direction energy (W) incident on the emission surface falls within dW per second per unit area, can be formulated analytically as [20]

$$N(W)dW = \frac{4\pi}{h^3}\left[\int_0^{\infty} f(W,\rho)\rho d\rho\right]dW = \frac{4\pi mkT}{h^3}\ln\left\{1+\exp\left[\frac{-(W-\zeta)}{kT}\right]\right\}dW \tag{5}$$

where h is Planck's constant, ρ is the radial electron momentum (perpendicular to the emission direction), k is Boltzmann's constant, T is the emitter temperature, ζ is the Fermi level (see Fig. 2), and $f(W,\rho)$ is the Fermi-Dirac function:

$$f(W,\rho) = \frac{1}{\exp\left(\frac{W-\zeta}{kT} + \frac{\rho^2}{2mkT}\right)+1}. \tag{6}$$

Several simplifying assumptions have been invoked historically to reduce the integral in Eq. (3) to an analytic form. As described above, the use of the field enhancement factor β linearizes the first term of Eq. (1) as $-q\beta Fx$. Also, the temperature dependence is eliminated by neglecting the spreading of the Fermi-Dirac function with increasing temperature. With these assumptions and other integration approximations [20], the current density integral can be expressed analytically as:

$$J = \frac{1.5\times10^{-6}\beta^2F^2}{\phi}\exp\left(\frac{10.4}{\phi^{1/2}}\right)\exp\left(\frac{-6.44\times10^7\phi^{3/2}}{\beta F}\right) \tag{7}$$

where J is the average current density (A/cm^2), F is the *average* applied electric field (V/cm), and ϕ is an effective work function (eV). The foregoing equation is the basic Fowler-Nordheim relation for field emission current. Note that temperature effects are absent. However, most experimental data for room-temperature emission exhibit reasonable agreement with the Fowler-Nordheim theory.

Experimental data are often plotted in so-called Fowler-Nordheim coordinates to determine unknown or uncertain parameters such as emission area, work function, and field enhancement factor by rearranging Eq. (7) as

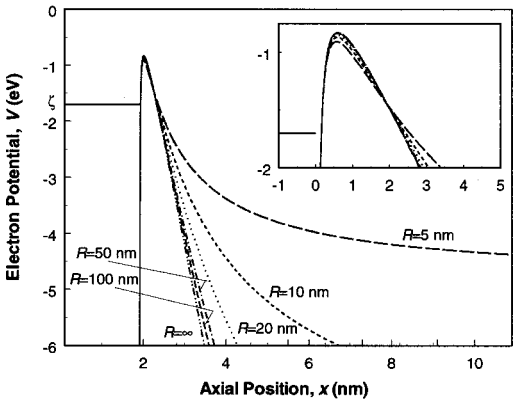

Fig. 3 Electron potential as a function of position from emitter and emitter radius. All profiles produce the same current density, $J = 10$ A/cm^2. $\phi = 1.7$ eV. $K = 5.5$. $T = 300$ K.

$$\ln\left(\frac{I}{F^2}\right) = C_0(A,\beta,\phi) + C_1(\beta,\phi)\frac{1}{F} \tag{8}$$

where I is the measured current, and A is the effective emission area. A linear fit of F^1 versus $\ln(I/F^2)$ enables the evaluation of the two constants C_0 and C_1, which depend on area A, field enhancement factor β, and effective work function ϕ. Thus, the formulation is underdetermined, and an assumed value is typically taken for one of the three primary variables. As discussed later, significant opportunities for advanced techniques, such as parameter estimation, exist for interpreting experimental data.

The emitter's radius R has a profound effect on the field required to produce emission. Figure 3 shows the potential field near the emitter for radii ranging from $R=5$ nm to infinity (i.e., a planar surface). We choose an effective work function of $\phi=1.7$ eV and a dielectric constant $K=5.5$ (i.e., that of diamond). The value of the work function is a convenient choice to demonstrate energy conversion processes. This choice is consistent with the minimum Schottky barrier for nitrogen-doped diamond [32] and with recent observations and analysis of emission from graphite-like grain boundary regions [43,44]. Later, results for several values of work function are considered (see Fig. 5). For each curve in Fig. 3, the average field produces a current density of 10 A/cm^2, as computed using the potential profile of Eq. (1) and numerical evaluations of the current density integral in Eq. (3). We note that the potential curves for emitter radii smaller than 50 nm exhibit large differences, while those for radii greater than 50 nm (including the planar case $R=\infty$) are quite similar. The figure indicates that the barrier width is slightly narrower in the high-energy regions (i.e., above the Fermi level) for small radii and substantially larger at lower energies for small radii. Thus, the emission radius influences the energetic distribution of emission. The required applied (average) fields range from $F=1.08\ \mathrm{V}/\mu\mathrm{m}$ for $R=5$ nm to $F=614\ \mathrm{V}/\mu\mathrm{m}$ for a planar surface ($R=\infty$). This difference in applied field strongly influences energy conversion due to the increased losses (e.g., from higher required voltages) incurred at high fields.

2.3 Energy Transport. The starting point for energy transport modeling is the current density integral of Eq. (3), from which the number of electrons emitted per unit time and area can be derived. Energy moments of this integral can provide energy transport rates. Chung et al. [27] reported related calculations for overall electron energy using numerical evaluation of double integrals. Here, we separate energy into axial (i.e., in the emission direction) and radial (i.e., perpendicular to the emission direction) components. The underlying free-electron model of the emitter material and the separability of the potential field employed here permit this spatial separation. The advantages of the present formulation are that (1) the double integral can be reduced analytically to a single integral and (2) directional information is retained that is useful in studying important problems that result from electron deposition in the gate or anode. For example, modeling and simulation of anode heating in field emission electronic devices requires an understanding of both the spatial and energetic distributions of electron energy emitted from the cathode.

The average total energy of emitted electrons can be expressed as the sum of axial and radial components, $\langle\varepsilon\rangle=\langle W\rangle+\langle\varepsilon_\rho\rangle$. The average axial energy can be calculated as

$$\langle W\rangle = \frac{1}{J}\int_{-W_a}^{\infty} qWD(W)N(W)dW \tag{9}$$

where the transmission function $D(W)$ and the supply function $N(W)dW$ are given in Eqs. (3) and (4), respectively. Similarly, the radial component becomes

$$\begin{aligned}\langle\varepsilon_\rho\rangle &= \frac{4\pi q}{Jh^3}\int_{-W_a}^{\infty}\int_0^{\infty} D(W)f(W,\rho)\frac{\rho^3}{2m}d\rho dW \\ &= \frac{4\pi qm(kT)^2}{Jh^3}\int_{-W_a}^{\infty} D(W) \\ &\quad\times\left(\frac{1}{2}\alpha(W)^2+\frac{\pi^2}{6}+\mathrm{dilog}[e^{\alpha(W)}+1]\right)dW\end{aligned} \tag{10}$$

where

$$\alpha(W) = \frac{W-\zeta}{kT} \tag{11}$$

$$\mathrm{dilog}(x) = \int_1^x \frac{\ln(t)}{1-t}dt. \tag{12}$$

The dilog function can be computed efficiently as a series [45].

The sum of the axial and radial energies of Eqs. (9) and (10) represents the total average energy of emitted electrons. These electrons must be replaced by others to preserve charge continuity. The difference in total average energy between emitted and replacement electrons determines whether field emission produces heating or cooling of the cathode. For example, if the average emitted energy exceeds the average replacement energy, then cooling ensues (neglecting other possible energy transport mechanisms, such as reverse emission). The energies of replacement electrons typically fall near the chemical potential ζ. Chung et al. [27] and Cutler et al. [28] showed that the average energy of replacement electrons can be several tenths of an electron volt below ζ. Again, the present formulation differs from that of Chung et al. by separating the axial and radial energy components. The average axial ($\langle W_r\rangle$) and radial ($\langle\varepsilon_{\rho r}\rangle$) replacement energies can be expressed as an integral over available energy states below the chemical potential as

$$\begin{aligned}\langle W_r\rangle &= \int_{-W_a}^{\zeta}\int_0^{\zeta-W} W\{1-f(W,\rho)[1-D(W)]\}d\varepsilon_\rho dW \Big/ \int_{-W_a}^{\zeta}\int_0^{\zeta-W}\{1-f(W,\rho)[1-D(W)]\}d\varepsilon_\rho dW \\ &= \frac{\int_{-W_a}^{\zeta} W\{(\zeta-W)+[1-D(W)]kT\}[\ln 2+\alpha(W)-\ln[e^{\alpha(W)}+1]]dW}{\int_{-W_a}^{\zeta}\{(\zeta-W)+[1-D(W)]kT\}[\ln 2+\alpha(W)-\ln[e^{\alpha(W)}+1]]dW}\end{aligned} \tag{13}$$

$$\langle\varepsilon_{\rho r}\rangle = \frac{\int_{-W_a}^{\zeta}\int_0^{\zeta-W}\varepsilon_\rho\{1-f(W,\rho)[1-D(W)]\}d\varepsilon_\rho dW}{\int_{-W_a}^{\zeta}\int_0^{\zeta-W}\{1-f(W,\rho)[1-D(W)]\}d\varepsilon_\rho dW} = \frac{\int_{-W_a}^{\zeta} g(W)dW}{\int_{-W_a}^{\zeta}\{(\zeta-W)+[1-D(W)]kT\}[\ln 2+\alpha(W)-\ln[e^{\alpha(W)}+1]]dW} \tag{14}$$

where

$$g(W)=\frac{(\zeta-W)^2}{2}-[1-D(W)](kT)^2\left\{\frac{\pi^2}{12}-\ln(2)\alpha(W)+\frac{1}{2}\alpha(W)^2+\mathrm{dilog}[e^{\alpha(W)}+1]\right\}. \quad (15)$$

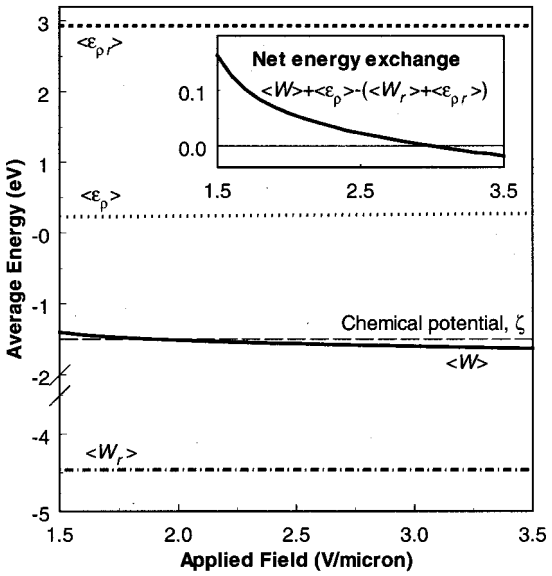

Fig. 4 Average emitted and replacement electron energies as a function applied field. Average axial emitted energy=$\langle W\rangle$. Average radial emitted energy $\langle\varepsilon_\rho\rangle$. Average axial replacement energy=$\langle W_r\rangle$. Average radial emitted energy $\langle\varepsilon_{\rho r}\rangle$. Figure inset shows net electron exchange energy as a function of applied field. Emitter characteristic radius R=10 nm. Work function ϕ=1.7 eV. K=5.5. Temperature T=300 K.

Each of the integrals in Eqs. (3), (9), (10), (13), and (14) has been evaluated numerically with adaptive quadrature to a convergence to five decimal places. The combination of these integrals provides a means of evaluating the rate of energy flux q'' to or from the cathode due to electron emission. This energy flux can be expressed as the product of the electrical current density and the difference in average energy between emitted and replacement electrons:

$$q''=\frac{J}{q}[\langle W\rangle+\langle\varepsilon_\rho\rangle-(\langle W_r\rangle+\langle\varepsilon_{\rho r}\rangle)]. \quad (16)$$

The average energies described above depend on the applied field F, as shown in Figure 4 for an effective emitter radius of $R=10$ nm at a temperature $T=300$ K. For low fields, the average axial emission energies $\langle W\rangle$ are relatively high compared to the lowest possible axial energy. As the field increases, the energy decreases. The decrease in the emission energy is a consequence of the narrowing barrier width at highly populated energy states. For both axial ($\langle W_r\rangle$) and transverse ($\langle\varepsilon_{\rho r}\rangle$) replacement energies, the slight decrease in energy is a consequence of the greater number of empty low-energy states due to emission from those states. In the case of emission electrons, their average transverse energies ($\langle\varepsilon_\rho\rangle$), which must be greater than zero, tend to increase with increasing field due to the reduction in axial energies described above. This increase is a consequence of the distribution of directional energies governed by Fermi-Dirac statistics (i.e., as axial energy decreases, higher radial energy states become available). The inset of Fig. 4 shows the net electron energy exchange due to the foregoing mechanisms. The net exchange is positive at low field due primarily to the emission of high-energy electrons through the top of the potential barrier. As the field increases,

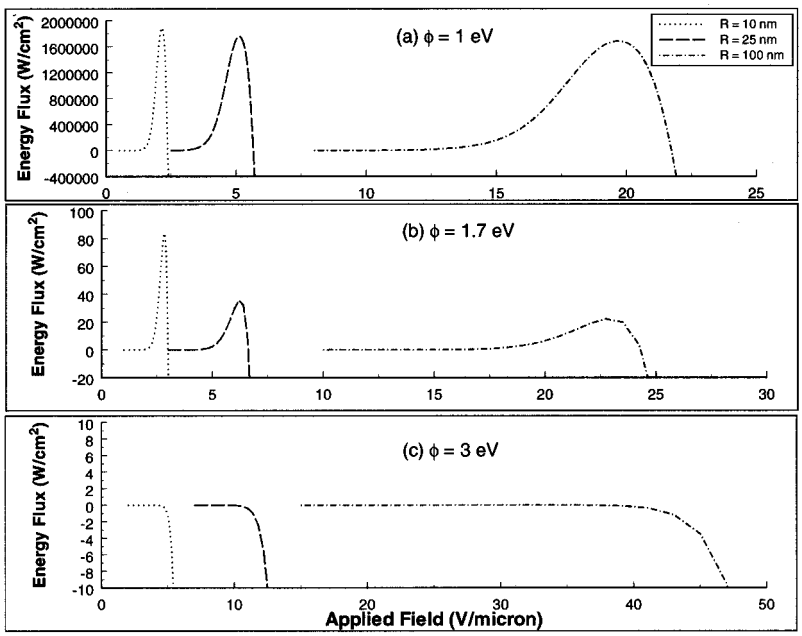

Fig. 5 Emission energy flux from the cathode as a function applied field F, emitter characteristic radius R, and work function ϕ: (*a*) ϕ=1 eV; (*b*) ϕ=1.7 eV; and (*c*) ϕ=3 eV. Each part shows curves for three emitter radii, R=10, 25, and 100 nm. K=5.5. Temperature T=300 K.

more low-energy electrons emit, and at a field of approximately 3 V/μm, the net exchange of energy becomes negative and causes cathode heating.

Predictions from the theory outlined above suggest that substantial rates of direct electrical-thermal energy conversion and transfer are possible with field emission. The energy flux q'' from the cathode depends primarily on four parameters: (1) emitter work function ϕ, (2) characteristic emitter radius R, (3) applied field F, and (4) temperature T. As shown in Fig. 4, net exchange energies greater than 0.1 eV are possible. The net energy flux is the product of this exchange energy and the electric current density [see Eq. (16)], and consequently, even a large net energy exchange may produce little thermodynamic effect if the current density is low.

Figure 5 shows the results of this balance for three emitter radii ($R=10$ nm, 25 nm, 100 nm) and work functions ($\phi=1$ eV, 1.7 eV, 3 eV). For each condition, the energy flux at low fields is negligible due to the low electrical current density. As the field increases, the electrical current increases, and substantial energy flux away from the emitter is made possible by the net energy exchange between emitted and replacement electrons. As the field increases further, the energy exchange decreases and ultimately becomes negative, which causes heating. As the emitter radius increases, the peak energy flux decreases due to the downward shift in energy distribution that is inherent to larger radii (see Fig. 2). At the same time, the field range for positive energy flux grows with increasing radius due to the reduction in field enhancement. The figure also shows a strong influence of the work function. For the lowest work function, $\phi=1$ eV, very high rates of local energy flux of order $q''\sim 10^6$ W/cm^2 are predicted for all emitter radii. The corresponding local current densities for the maximum energy fluxes are of order $J\sim 10^7$ A/cm^2 for all radii. As the work function increases to $\phi=1.7$ eV, the peak energy fluxes decrease significantly ($q''\sim 10$ to 100 W/cm^2), and local current densities at the peak energy fluxes are of order $J\sim 10^4$ A/cm^2. For the largest work function, $\phi=3$ eV, maximization of energy flux is not evident, and the energy flux is negligible or negative over the entire range of applied fields. These results indicate that low-work-function materials are necessary to enable significant energy conversion. The probability of developing materials with effective work functions as low as $\phi=1$ eV are quite remote, and therefore the associated heat fluxes in Fig. 1(a) may be practically infeasible. For the case of semiconductor emitters, appropriate n-type dopants could potentially produce effective work functions near $\phi=1.7$ eV, and we note that, in the particular case of diamond, the goal of finding suitable shallow donors has been elusive. However, several recent studies indicate some optimism in this area [46–49].

3 Discussion

Field emission from semiconductor materials can involve both internal emission from a metallic conductor into the semiconductor and external emission from the semiconductor into vacuum. For example, much recent work [32–34,50,51] on diamond emitters suggests that the interface between a base electrode (either metallic or semiconductor) and diamond (a wide-bandgap semiconductor) governs the field emission process. Therefore, the analysis of semiconductor emitters can be substantially more complicated than that of metals (such as shown in Fig. 2). However, wide-bandgap semiconductors, such as diamond, can provide substantial energy filtering effects as well as favorable structural properties, and consequently, are well suited to direct energy conversion applications.

Tunneling into the conduction band of a diamond cathode is shown schematically in the one-dimensional band diagrams of Fig. 6. Figure 6(a) shows the unbiased state, with slight band bending due to space charge effects [52]. The band gap, $E_g=E_C-E_V$, of diamond is 5.5 eV, and the difference between the base electrode's Fermi energy and the cathode's valence band energy for an undoped sample is $E_{FB}-E_V=1.4$ eV, which is the energy associated with grain boundaries. Cathode doping can alter this energy difference. The effective work function ϕ_{eff} represents the axial electron energy required for an electron in the base electrode to emit into vacuum. The parameter $\chi=E_{\text{vac}}-E_C$ is the electron affinity and represents the energy required to eject an electron from the conduction band into vacuum. Numerous recent studies indicate that χ is negative (although it is shown positive in Fig. 6) when the diamond surface is terminated by hydrogen [53–56]. This negative electron affinity can significantly enhance emission.

A gate electrode can be used to extract high-energy electrons from the cathode. Figure 1 shows nanotip emitters surrounded by gate structure. Under a voltage bias (positive on the gate electrode), the electric field causes the bands in the cathode and vacuum to shift, as shown in Fig. 6(b). Near the base-electrode/cathode interface, significant band bending narrows the potential barrier width. This narrow barrier increases the probability of quantum tunneling, and field emission occurs. A second tunneling process may also occur at the cathode/vacuum barrier for $\chi>0$.

The presence of internal field emission significantly complicates the task of modeling. Solid-state scattering events can alter the distribution of electrons that ultimately emit into vacuum. For polycrystalline diamond films near room temperature, Lerner et al. [31] showed that electrons can travel quasiballistically for films less than several microns in thickness. Thus, for thin films, the band structure of Fig. 6 can provide the basis for a reasonable emission model. However, neither Fowler-Nordheim theory nor the foregoing model possesses the fidelity to represent such complex profiles in detail. We note, however, that unlike basic Fowler-Nordheim theory, the present model does allow for the inclusion of size effects in thermodynamic calculations. A more rigorous approach generally requires numerical solutions to Schrödinger's equation [57], and the inclusion of multi-dimensional effects [58]. The numerical solution of Schrödinger's equation possesses the advantage of eliminating the WKB approximation in the evalua-

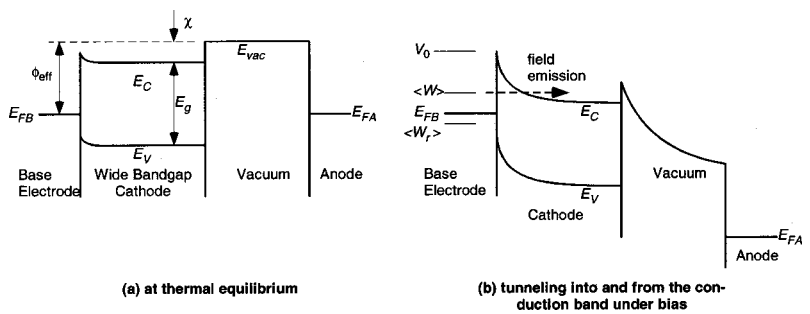

Fig. 6 Band diagrams for field emission from diamond: (*a*) Unbiased at thermal equilibrium; and (*b*) Field emission via tunneling from the base electrode to the cathode's conduction band and from the conduction band to vacuum

tion of transmission coefficients. Further, a general numerical solver would enable analysis of more complex systems, such as resonant-tunneling structures [6–8]. Advanced, multidimensional tunneling formulations have been reported [59–64] with particular application to scanning tunneling microscopy. However, to date, a combined analysis, including complex band structure, multi-dimensionality, numerically computed transmission coefficients, and energy exchange calculations has not been reported and would represent a significant achievement.

We also anticipate that, with recent and continued progress in nanoscale fabrication methods, new nanoscale materials and surfaces will require the replacement of continuum models with subcontinuum quantum models. Such models would replace the supply function $N(W)dW$ of Eq. (5). Miskovsky and co-workers have shown that discrete atomic-scale effects can strongly influence the local density of electron states from which emitting electrons originate [65]. They have also considered strong localized heating and thermoelectric effects near atomically sharp emitters [66]. Karabutov et al. [44] have postulated that two-dimensional quantum wells are responsible for the low turn-on fields of polycrystalline diamond emitters. Interestingly, the resulting current-voltage relations still closely follow Fowler-Nordheim trends. Fursey and Glazanov have compared current-voltage predictions of formulations that include nanoscale tip curvature with those from traditional Fowler-Nordheim theory [67]. A group of studies by He, Cutler, Miskovsky, and co-workers [68–71] and Jensen and co-workers [39,72] highlight the effects of nanoscale tip geometries on field emission and the commensurate shortcomings of using traditional Fowler-Nordheim theory for these small-scale devices. These studies reinforce the need for advanced treatment of nanoscale and atomic effects in the study of field emitters.

Advanced electron spectroscopy will be required to study rigorously the thermodynamics of field emission. Gadzuk and Plummer reviewed the field-emission energy distribution (FEED) technique [73]. Most such spectrometers employ hemispherical elements [74,75]. Recently, researchers have developed non-hemispherical [76] and simplified hemispherical [77] devices that offer enhanced resolution and simplicity. Electron spectroscopy has proven to be useful for studying field emission devices with electronic functions. An understanding of the electron energy distribution is particularly important in the study of anode heating, which is a significant cause of failure in high-current field emission devices [78]. For energy-conversion field-emission devices, experimental quantification of electron energy distributions will be essential.

Another area for further study involves the interpretation of experimental data and its comparison with increasingly complex models. Determination of emission parameters from the Fowler-Nordheim theory [see Eq. (7)] has historically been a heuristic process where the value of the parameters is largely dependent on the estimation procedure. The incongruous results are a feature of the models because the unknown parameters of interest are primarily non-physical and are, in general, correlated. The Fowler-Nordheim formulation of emission involves three parameters, namely the emission area (A), the work function (ϕ), and a field enhancement factor (β). However, by casting emission data into a linear form, only two parameters can be uniquely determined; two of the free parameters are linearly dependent on the third. As a result, experimenters must fix one of the free parameters using independent data and then proceed to estimate the remaining parameters using a linear regression.

One approach commonly used and described by Brodie and Schwoebel [13] is to differentiate the Fowler-Nordheim equation with respect to the applied voltage. The voltage and current are measured in experiments and the derivative of the $I-V$ characteristics can also be obtained from the data. Thus, at any point, a value for C_0 [see Eq. (8)] can be calculated, and a regression procedure is commonly employed to estimate its value. Substitution of this value back into the governing equation provides C_1. Estimates of these two factors enable estimation of two of the three unknown parameters (A, ϕ, and β) with an assumed value for the third. Estimation of these values is dubious with linear Fowler-Nordheim analysis. Also note that the estimation of the derivative of the data (dI/dV) deserves scrutiny because the differentiation of discrete points tends to magnify experimental errors [79].

A geometrically more rigorous approach to emission modeling and interpretation of experimental data has been developed by Jensen and co-workers [37,72,80]. In their work, the emission area and field enhancement are related analytically to the geometry of the tip emitter. Further, the variability of emission from multiple tips in an array is considered explicitly. It is likely that such an approach, when coupled with emission models that include band-bending effects, will provide greater efficacy in the interpretation of experiment results.

In all existing and proposed models for the interpretation of field emission data, a statistical approach can provide estimates with superior confidence as well as insights into the accuracy of estimated parameters. The sensitivity of the emission current to the free parameters can indicate the identifiability of the parameters in a given emission model. Parameter estimation techniques [81,82] represent a powerful tool for experimental interpretation and model development. Such tools are particularly suitable for field emission applications due to significant measurement noise (e.g., transient fluctuations of emission current) and the potential complexity of new theoretical and computational models. For example, the model developed herein, with the inclusion of temperature and characteristic emitter radius, presents an opportunity for more rigorous determination of physics-based emission parameters through advanced estimation methods.

The questions of total energy conversion capacity and efficiency are important to consider for the broad range of potential applications of field emission devices. The energy fluxes shown in Fig. 5 result from emission from nanoscale emitters. Both the local energy flux and the number density per unit area of nanoscale emitters will ultimately determine the total energy conversion capacity. A variety of fabrication technologies-nanodiamond pyramidal tips [83], focused ion beam molds [84], and carbon nanotubes [85]-exist that can produce tremendously high number densities of field nanoemitters. We believe that the rapidly evolving field of nanofabrication will ultimately present a wide range of fabrication options.

Ideally, the thermodynamic performance metrics, coefficient of performance for refrigeration and thermal efficiency for power generation, of field emission devices should approach that of the limiting Carnot efficiency, in a manner similar to that of vacuum thermionic devices [86]. In practice, thermal radiation and conduction losses, as well as electrical losses (e.g., in terminal leads and from Joule heating of tip emitters), would limit practical maximum efficiencies to approximately 50–70 percent of the Carnot efficiencies. This estimate is consistent with those for thermionic converters [86]. Calculations by Cutler et al. [10] suggest that the coefficient of performance of a refrigeration field emission device can exceed that of traditional thermoelectric devices. The performance can improve further through the use of gate electrodes and with retarding potentials. For power generation applications, traditional thermionic devices using metallic emitters can be highly efficient. However, the use of these materials has been limited to high temperature ($>$1500 K) applications because they prevent the emission of all except the highest energy electrons. In effect, thermionic converters are limited by the emitter material's work function. In contrast, the development of novel emitter materials with low work functions could make the thermionic process amenable to operation at lower temperatures due to the allowed emission of lower-energy electrons. Consequently, we believe that field emission materials and devices hold great promise for enabling the operation of a fundamentally efficient energy

conversion mechanism in temperature ranges where other direct energy conversion processes lack either sufficient capacity (e.g., thermionics) or efficiency (e.g., thermoelectrics).

4 Summary and Conclusions

Field emission offers an intriguing new technical approach for direct energy conversion. This work has provided an overview of the physics of electron field emission with particular emphasis on thermal and nanoscale geometric effects. The traditional model for field emission, based on Fowler-Nordheim theory, ignores thermal effects and linearizes highly non-linear fields in order to achieve an analytic solution. The new model presented herein includes the effects of temperature and nanoscale emitter geometry. The efficacy of this approach is demonstrated by the strong effects of the characteristic emitter radius on emission (see Figs. 3 and 5).

The potential for high energy capacity and high efficiency suggests that field emission devices may find a broad range of applications; however, many technical challenges remain, particularly as new nanoscale materials and fabrication technologies emerge. As characteristic dimensions decrease below 10 nm, the continuum assumption becomes suspect, and atomic-scale modeling will be required. Further, the complex band structure of semiconductor emitters, even at continuum scales, necessitates more advanced approaches to the characterization of quantum tunneling. In order for models to be useful, important material properties, such as work functions and electron affinities, must be characterized experimentally.

Another major challenge lies in the demonstration of practical energy conversion. In order to serve useful engineering purposes, the nanoscale emission phenomenon must be scaled up to macroscopic dimensions. Thus geometric, chemical, and surface uniformity will be important considerations in any functional device. The achievement of such uniformity is a significant challenge, even in a laboratory setting.

Finally, we note that a complete study of practical thermodynamic efficiencies has not yet been reported. The similarity between field emission and thermionic emission suggests that high efficiency operation is possible. The efficiency will depend on a wide range of factors, including radiative material properties, anode work functions, and electrical resistivity of electrodes. This issue is the subject of current study by the authors.

Acknowledgments

The authors thank Professors J. L. Davidson, W. P. Kang, and A. M. Strauss for helpful conversations. This work was supported by the NSF CAREER program (Grant # CTS-9983961) and by a Vanderbilt Discovery Grant.

Nomenclature

$D(W)$ = tunneling transmission coefficient, see Eq. (4)
F = applied electric field $(V/\mu\text{m}) = V/L$
f = Fermi-Dirac function, see Eq. (6)
$G(x)$ = image charge potential (V), see Eq. (2)
h = Planck's constant $= 4.1357 \times 10^{-15}$ eV·s
I = electrical current (A)
J = current density (A/cm^2)
K = emitter's dielectric constant
k = Boltzmann's constant $= 8.617 \times 10^{-5}$ eV/K
L = cathode-anode separation (μm)
m = electron rest mass $= 9.1095 \times 10^{-31}$ kg
$N(W)$ = electron supply function [s/(kg m^4)], see Eq. (5)
q = electron charge $= 1.60219 \times 10^{-19}$ Coulomb
R = emitter characteristic radius (nm)
V = applied voltage (V)
W = axial electron energy (eV)
x = axial coordinate (m)

Greek Symbols

β = field enhancement factor, see Fig. 2
χ = electron affinity (eV), see Fig. 6
ε = dielectric constant, see Eq. (2)
ϕ = work function (eV), see Fig. 2
ζ = Fermi level (eV), see Fig. 2
ρ = radial electron momentum (kg m/s)

Subscripts

r = replacement electron value
ρ = radial direction

References

[1] Hicks, L. D., and Dresselhaus, M. S., 1993, ''Effect of Quantum-Well Structures on the Thermoelectric Figure of Merit,'' Phys. Rev. B, **47**, pp. 12 727–12 731.
[2] Mahan, G. D., 1998, ''Good Thermoelectrics,'' Solid State Phys., **51**, pp. 81–157.
[3] Mahan, G. D., and Woods, L. M., 1998, ''Multilayer Thermionic Refrigeration,'' Phys. Rev. Lett., **18**, pp. 4016–4019.
[4] Shakouri, A., Lee, E. Y., Smith, D. L., Narayanamurti, V., and Bowers, J. E., 1998, ''Thermoelectric Effects in Submicron Heterostructure Barriers,'' Microscale Thermophys. Eng., **2**, pp. 37–47.
[5] Miskovsky, N. M., and Cutler, P. H., 1999, ''Microelectronic Cooling Using the Nottingham Effect and Internal Field Emission in a Diamond (Wide-Band Gap Material) Thin-Film Device,'' Appl. Phys. Lett., **75**, pp. 2147–2149.
[6] Tsu, R., and Greene, R. F., 1999, ''Inverse Nottingham Effect Cooling in Semiconductors,'' Electrochem. Solid-State Lett., **2**, pp. 645–647.
[7] Korotkov, A. N., and Likharev, K. K., 1999, ''Possible Cooling by Resonant Fowler-Nordheim Emission,'' Appl. Phys. Lett., **75**, pp. 2491–2493.
[8] Korotkov, A. N., and Likarev, K. K., 2000, ''Cooling by Resonant Fowler-Nordheim Emission,'' Physica B, **284**, pp. 2030–2031.
[9] Fisher, T. S., 2001, ''Influence of Nanoscale Geometry on the Thermodynamics of Electron Field Emission,'' Appl. Phys. Lett., **79**(22), pp. 3699–3701.
[10] Cutler, P. H., Miskovsky, N. M., Kumar, N., and Chung, M. S., 2000, ''New Results on Microelectronic Cooling Using the Inverse Nottingham Effect. Low Temperature Operation and Efficiency,'' Electrochemical Society Proceedings, **2000–28**, pp. 99–111.
[11] Fowler, R. H., and Nordheim, L. W., 1928, ''Field Emission From Metallic Surfaces,'' Proc. R. Soc. London, Ser. A, **119**, pp. 173–181.
[12] Spindt, C. A., 1968, ''A Thin Film Field Emission Cathode,'' J. Appl. Phys., **39**, pp. 3504–3505.
[13] Brodie, I., and Schwoebel, P. R., 1994, ''Vacuum Microelectronic Devices,'' Proc. IEEE, **82**, pp. 1006–1018.
[14] Nation, J. A., Schachter, L., Mako, F. M., Len, L. K., Peter, W., Tang, C.-M., and Rao, T., 1999, ''Advances in Cold Cathode Physics and Technology,'' Proc. IEEE, **87**, pp. 865–889.
[15] Kang, W. P., Fisher, T. S., and Davidson, J. L., 2001, ''Diamond Microemitters—The New Frontier of Electron Field Emission and Beyond,'' New Diamond and Frontier Carbon Technology, **11**, pp. 129–146.
[16] Robertson, J., 1999, ''Mechanisms of Electron Field Emission from Diamond, Diamond-Like Carbon, and Nanostructured Carbon,'' J. Vac. Sci. Technol. B, **17**, p. 659.
[17] Fleming, G. M., and Henderson, J. E., 1940, ''The Energy Losses Attending Field Current and Thermionic Emission of Electrons from Metals,'' Phys. Rev., **58**, pp. 887–894.
[18] Nottingham, W. B., 1941, ''Remarks on Energy Losses Attending Thermionic Emission of Electrons from Metals,'' Phys. Rev., **59**, pp. 906–907.
[19] Fleming, G. M., and Henderson, J. E., 1941, ''On the Energy Losses Attending Thermionic and Field Emission,'' Phys. Rev., **59**, pp. 907–908.
[20] Good, R. H., and Muller, E. W., 1956, ''Field Emission,'' Handbook of Physics, **21**, pp. 176–231.
[21] Dyke, W. P., and Dolan, W. W., 1956, ''Field Emission,'' Adv. Electron. Electron Phys., **VIII**, pp. 90–187.
[22] Gomer, R., 1961, *Field Emission and Field Ionization*, Harvard University Press, Cambridge, MA.
[23] Swanson, L. W., Crouser, L. C., and Charbonnier, F. M., 1966, ''Energy Exchanges Attending Field Electron Emission,'' Phys. Rev., **151**, pp. 327–340.
[24] Engle, I., and Cutler, P. H., 1967, ''The Effect of Different Surface Barrier Models on the Nottingham Energy Exchange Process,'' Surf. Sci., **8**, pp. 288–307.
[25] Bergeret, H., Septier, A., and Drechsler, M., 1985, ''Nottingham Effect of a Superconducting Metal,'' Phys. Rev. B, **31**, pp. 149–153.
[26] Miskovsky, N. M., Park, S. H., He, J., and Cutler, P. H., 1993, ''Energy Exchange Processes in Field Emission from Atomically Sharp Metallic Emitters,'' J. Vac. Sci. Technol. B, **11**, pp. 366–370.
[27] Chung, M. S., Cutler, P. H., Miskovsky, N. M., and Sullivan, T. E., 1994, ''Energy Exchange Processes in Electron Emission at High Fields and Temperatures,'' J. Vac. Sci. Technol. B, **12**, pp. 727–736.
[28] Cutler, P. H., Chung, M. S., Miskovsky, N. M., Sullivan, T. E., and Weiss, B. L., 1994, ''A New Model for the Replacement Process in Electron-Emission at High Fields and Temperatures,'' Appl. Surf. Sci., **76**, pp. 1–6.
[29] Huang, Z.-H., Cutler, P. H., Miskovsky, N. M., and Sullivan, T. E., 1995,

''Calculation of Electron Field Emission from Diamond Surfaces,'' J. Vac. Sci. Technol. B, **13**, pp. 526–530.
[30] Cutler, P. H., Huang, Z.-H., Miskovsky, N. M., D'Ambrosio, P., and Chung, M., 1996, ''Monte Carlo Study of Hot Electron and Ballistic Transport in Diamond: Low Electric Field Region,'' J. Vac. Sci. Technol. B, **14**, pp. 2020–2023.
[31] Lerner, P., Cutler, P. H., and Miskovsky, N. M., 1997, ''Hot Electron and Quasiballistic Transport of Nonequilibrium Electrons in Diamond Thin Films,'' J. Vac. Sci. Technol. B, **15**, pp. 398–400.
[32] Lerner, P., Cutler, P. H., and Miskovsky, N. M., 1997, ''Theoretical Analysis of Field Emission from a Metal Diamond Cold Cathode Emitter,'' J. Vac. Sci. Technol. B, **15**, pp. 337–342.
[33] Lerner, P., Miskovsky, N. M., and Cutler, P. H., 1998, ''Model Calculations of Internal Field Emission and J-V Characteristics of a Composite n-Si and N-Diamond Cold Cathode Source,'' J. Vac. Sci. Technol. B, **16**, pp. 900–905.
[34] Cutler, P. H., Miskovsky, N. M., Lerner, P. B., and Chung, M. S., 1999, ''The Use of Internal Field Emission to Inject Electronic Charge Carriers into the Conduction Band of Diamond Films: A Review,'' Appl. Surf. Sci., **146**, pp. 126–133.
[35] Everhart, T. E., 1967, ''Simplified Analysis of Point-Cathode Electron Sources,'' J. Appl. Phys., **38**, pp. 4944–4957.
[36] Robinett, R. W., 1997, *Quantum Mechanics: Classical Results, Modern Systems, and Visualized Examples*, Oxford University Press, New York, pp. 263–264.
[37] Jensen, K. L., Kodis, M. A., Murphy, R. A., and Zaidman, E. G., 1997, ''Space Charge Effects on the Current-Voltage Characteristics of Gated Field Emitter Arrays,'' J. Appl. Phys., **82**, pp. 845–854.
[38] Modinos, A., 1984, *Field, Thermionic and Secondary Electron Emission Spectroscopy*, Plenum Press, New York.
[39] Jensen, K. L., and Zaidman, E. G., 1993, ''Field Emission from an Elliptical Boss: Exact Versus Approximate Treatments,'' Appl. Phys. Lett., **63**, pp. 702–704.
[40] Jensen, K. L., 1999, ''Semianalytical Model of Electron Source Potential Barriers,'' J. Vac. Sci. Technol. B, **17**, pp. 515–519.
[41] Nazarov, Yu. V., 1989, ''Anomalous Current-Voltage Characteristics of Tunnel Junctions,'' Sov. Phys. J., **68**, pp. 561–566.
[42] Robinett, R. W., 1997, *Quantum Mechanics: Classical Results, Modern Systems, and Visualized Examples*, Oxford University Press, New York, pp. 229–233.
[43] Karabutov, A. V., Frolov, V. D., Pimenov, S. M., and Konov, V. I., 1999, ''Grain Boundary Field Electron Emission from CVD Diamond Films,'' Diamond Relat. Mater., **8**, pp. 763–767.
[44] Karabutov, A. V., Frolov, V. D., and Konov, V. I., 2001, ''Diamond/sp^2-Bonded Carbon Structures: Quantum Well Field Electron Emission,'' Diamond Relat. Mater., **10**, pp. 840–846.
[45] Dwight, H. B., 1961, *Tables of Integrals and Other Mathematical Data*, Macmillan Company, New York, p. 144.
[46] Collins, A. T., 1994, *Properties and Growth of Diamond*, G. Davies, ed., EMIS Datareviews Series No. 9, INSPEC, London.
[47] Koizumi, S., Kamo, M., Sato, Y., Mita, S., Sawabe, A., Reznik, A., Uzan-Saguy, C., and Kalish, R., 1998, ''Growth and Characterization of Phosphorus Doped *n*-type Diamond Thin Films,'' Diamond Relat. Mater., **7**, pp. 540–544.
[48] Sakaguci, I., Gamo, M. N., Kikuchi, Y., Yasu, E., and Haneda, H., 1999, ''Sulfur: A Donor Dopant for n-type Diamond Semiconductors,'' Phys. Rev. B, **60**, pp. R2139–R2141.
[49] Saada, D., Adler, J., and Kalish, R., 2000, ''Sulfur: A Potential Donor in Diamond,'' Appl. Phys. Lett., **77**, pp. 878–879.
[50] Geis, M. W., Twichell, J. W., and Lyszczarz, T. M., 1996, ''Diamond Emitters Fabrication and Theory,'' J. Vac. Sci. Technol. B, **14**, pp. 2060–2067.
[51] Koenigsfeld, N., Philosoph, B., and Kalish, R., 2000, ''Field Emission Controlled by the Substrate/CVD Diamond Interface,'' Diamond Relat. Mater., **9**, pp. 1218–1221.
[52] Silva, S. R. P., Amaratunga, G. A. J., and Okano, K., 1999, ''Modeling of the Electron Field Emission Process in Polycrystalline Diamond and Diamond-like Carbon Thin Films,'' J. Vac. Sci. Technol. B, **17**, pp. 557–561.
[53] Ristein, J., Stein, W., and Ley, L., 1998, ''Photoelectron Yield Spectroscopy on Negative Electron Affinity Diamond Surfaces: A Contactless Unipolar Transport Experiment,'' Diamond Relat. Mater., **7**, pp. 626–631.
[54] Baumann, P. K., and Nemanich, R. J., 1998, ''Surface Cleaning, Electronic States and Electron Affinity of Diamond (100), (111) and (110) Surfaces,'' Surf. Sci., **409**, pp. 320–355.
[55] Krainsky, I. L., and Asnin, V. M., 1998, ''Negative Electron Affinity Mechanism for Diamond Surfaces,'' Appl. Phys. Lett., **72**, pp. 2574–2576.
[56] Nemanich, R. J., Baumann, P. K., Benjamin, M. C., Nam, O.-H., Sowers, A. T., Ward, B. L., Ade, H., and Davis, R. F., 1998, ''Electron Emission Properties of Crystalline Diamond and III-Nitride Surfaces,'' Appl. Surf. Sci., **130**, pp. 694–703.
[57] Lui, W. W., and Fukuma, M., 1986, ''Exact Solution of the Schrödinger Equation Across an Arbitrary One-Dimensional Piecewise-Linear Potential Barrier,'' J. Appl. Phys., **60**, pp. 1555–1559.
[58] Fonseca, L. R. C., von Allmen, P., and Ramprasad, R., 2000, ''Numerical Simulation of the Tunneling Current and Ballistic Electron Effects in Field Emission Devices,'' J. Appl. Phys., **87**, pp. 2533–2541.
[59] Lang, N. D., 1985, ''Vacuum Tunneling Current from an Adsorbed Atom,'' Phys. Rev. Lett., **55**, pp. 230–233.
[60] Lang, N. D., 1986, ''Theory of Single-Atom Imaging in the Scanning Tunneling Microscope,'' Phys. Rev. Lett., **56**, pp. 1164–1167.
[61] Lang, N. D., 1986, ''Spectroscopy of Single Atoms in the Scanning Tunneling Microscope,'' Phys. Rev. B, **34**, pp. 5947–5950.
[62] Lucas, A. A., Morawitz, H., Henry, G. R., Vigneron, J.-P., Lambin, Ph., Cutler, P. H., and Feuchtwang, T. E., 1988, ''Scattering-Theoretic Approach to Elastic One-Electron Tunneling Through Localized Barriers: Application to Scanning Tunneling Microscopy,'' Phys. Rev. B, **37**, pp. 10 708–10 720.
[63] Lucas, A. A., Morawitz, H., Henry, G. R., Vigneron, J.-P., Lambin, Ph., Cutler, P. H., and Feuchtwang, T. E., 1988, ''Tunneling through Localized Barriers with Application to Scanning Tunneling Microscopy: New Scattering Theoretic Approach and Results,'' J. Vac. Sci. Technol. A, **6**, pp. 296–299.
[64] Huang, Z. H., Feuchtwang, T. E., Cutler, P. H., and Kazes, E., 1990, ''The Wentzel-Kramers-Brillouin Method in Multidimensional Tunneling: Application to Scanning Tunneling Microscopy,'' J. Vac. Sci. Technol. A, **8**, pp. 177–181.
[65] Miskovsky, N. M., and Cutler, P. H., 1999, ''Calculation of the Local Density of States for a Discrete Pyramidal Model of a Diamond Tip Surmounted by a Single Atom,'' Surf. Sci., **439**, pp. 173–180.
[66] Miskovsky, N. M., Park, S. H., He, J., and Cutler, P. H., 1993, ''Energy Exchange Processes in Field Emission from Atomically Sharp Metallic Emitters,'' J. Vac. Sci. Technol. B, **11**, pp. 366–370.
[67] Fursey, G. N., and Glazanov, D. V., 1998, ''Deviations from the Fowler-Nordheim Theory and Peculiarities of Field Electron Emission from Small-Scale Objects,'' J. Vac. Sci. Technol. B, **16**, pp. 910–915.
[68] He, J., Cutler, P. H., Miskovsky, N. M., and Feuchtwang, T. E., 1991, ''Derivation of the Image Interaction for Non-Planar Pointed Emitter Geometries: Application to Field Emission I-V Characteristics,'' Surf. Sci., **246**, pp. 348–364.
[69] He, J., Cutler, P. H., and Miskovsky, N. M., 1991, ''Generalization of Fowler-Nordheim Field Emission Theory for Nonplanar Metal Emitters,'' Appl. Phys. Lett., **59**, pp. 1644–1646.
[70] Cutler, P. H., He, J., and Miskovsky, N. M., 1993, ''Theory of Electron Emission in High Fields from Atomically Sharp Emitters: Validity of the Fowler-Nordheim Equation,'' J. Vac. Sci. Technol. B, **11**, pp. 387–391.
[71] Cutler, P. H., He, J., Miller, J., Miskovsky, N. M., Weiss, B., and Sullivan, T. E., 1993, ''Theory of Electron Emission in High Fields from Atomically Sharp Emitters: Validity of the Fowler-Nordheim Equation,'' Prog. Surf. Sci., **42**, pp. 169–185.
[72] Jensen, K. L., Mukhopadhyay-Phillips, P., Zaidman, E. G., Nguyen, K., Kodis, M. A., Malsawma, L., and Hor, C., 1997, ''Electron Emission from a Single Spindt-Type Filed Emitter: Comparison of Theory with Experiment,'' Appl. Surf. Sci., **111**, pp. 204–212.
[73] Gadzuk, J. W., and Plummer, E. W., 1973, ''Field-Emission Energy-Distribution (FEED),'' Rev. Mod. Phys., **45**, pp. 487–548.
[74] Kuyatt, C. E., and Simpson, J. A., 1967, ''Electron Monochromator Design,'' Rev. Sci. Instrum., **38**, pp. 103–111.
[75] Wysocki, J. K., 1982, ''Testing of a Field Electron Energy Analyser,'' Journal of Physics E-Scientific Instruments, **15**, pp. 1376–1385.
[76] Oshima, C., 1997, ''An Apparatus for High Resolution Field Emission Spectroscopy,'' Adv. Colloid Interface Sci., **71**, pp. 353–369.
[77] Bernhard, J. M., Rouse, A. A., Sosa, E. D., Gnade, B. E., Golden, D. E., and Chalamala, B. R., 1999, ''A Compact Electron Energy Analyzer for Measuring Field Emission Energy Distributions,'' Rev. Sci. Instrum., **70**, pp. 3299–3302.
[78] Grant, P., Py, C., Möbner, C., Blais, A., Tran, H., and Gao, M., 2000, ''Electron Field Emission From Diamond-like Carbon, a Correlation with Surface Modifications,'' J. Appl. Phys., **87**, pp. 1356–1360.
[79] Ehrich, F. F., 1954, ''Differentiation of Experimental Data Using Least Squares Fitting,'' J. Aeronaut. Sci., **22**, pp. 133–134.
[80] Jensen, K. L., Yater, J. E., Zaidman, E. G., Kodis, M. A., and Shih, A., 1998, ''Advanced Emitters for Next Generation RF Amplifiers,'' J. Vac. Sci. Technol. B, **16**, pp. 2038–2048.
[81] Beck, J. V., and Arnold, K. J., 1977, *Parameter Estimation in Engineering and Science*, Wiley, New York.
[82] Haftka, R. T., Scott, E. P., and Cruz, J. R., 1998, ''Optimization and Experiments: A Survey,'' Appl. Mech. Rev., **51**, pp. 435–448.
[83] Wisitsora-at, A., Kang, W. P., Davidson, J. L., Li, Q., Xu, J. F., and Kerns, D. V., 1999, ''Efficient Electron Emitter Utilizing Boron-Doped Diamond Tips with sp(2) Content,'' Appl. Surf. Sci., **146**, pp. 280–287.
[84] Gotoh, Y., Inoue, K., Ohtake, T., Ueda, H., Hishida, Y., Tsuji, H., and Ishikawa, J., 1994, ''Application of Focused Ion Beam Techniques to the Fabrication of Lateral-Type Thin-Film Edge Field Emitters,'' Japanese Journal of Applied Physics Part 2–Letters, **33**, pp. L63–L70.
[85] Tamtair, F. G., Chen, L. C., Wer, S. L., Hong, W. K., Chen, K. H., and Cheng, H. C., 2000, ''High Current Density Field Emission from Arrays of Carbon Nanotubes and Diamond-Clad Si Tips,'' J. Vac. Sci. Technol. B, **18**, pp. 1207–1213.
[86] Hatsopoulos, G. N., and Gyftopoulos, E. P., 1973, *Thermionic Energy Conversion*, Vol. I, MIT Press, Cambridge, MA, ch. 2.